ELSEVIER

Marine Geology 118 (1994) 119–137

MARINE GEOLOGY
INTERNATIONAL JOURNAL OF MARINE GEOLOGY, GEOCHEMISTRY AND GEOPHYSICS

Clastic components in Quaternary sediments of the northwest Pacific and their paleo-oceanic significance

Victor P. Nechaev[a], Anna V. Sorochinskaya[b], Ira B. Tsoy[b], Sergei A. Gorbarenko[b]

[a]*Far East Geological Institute, Far Eastern Branch, Russian Academy of Sciences, Vladivostok 690022, Russian Federation*

[b]*Pacific Oceanological Institute, Far Eastern Branch, Russian Academy of Sciences, Vladivostok 690032, Russian Federation*

(Received April 21, 1993; revision accepted August 23, 1993)

Abstract

Ninety-seven mineral analyses (for the total 0.05–0.1 mm fraction and its heavy subfraction) are given of Late Pleistocene to Holocene sediments from the northwestern (subarctic) Pacific, including the Kuril and Aleutian Trenches and Bering Sea. Heavy mineral assemblages indicating ice-rafted debris and its main provenance were defined. The assemblages are derived mainly from the northeastern Bering Sea shelf where large-scale generation of sea-ice is presumed. Temporal and spatial changes of the mineral suites also suggest intermediate to deep water flow along the eastern flank of the Emperor chain during glaciation. The flow might penetrate the Northwest Pacific Basin to the south of 45°N. It was traced by the fine- and medium-grained terrigenous debris in a core from 38°N and 165°E.

1. Introduction

The North Pacific, and its northwestern section in particular, is one of the best regions in which to study global changes in climate and ocean circulation based on Quaternary sediments. In part, this is because (1) the sediments often contain abundant microfossils (mainly diatomaceous and, to a lesser degree, radiolarian and foraminiferal) appropriate for paleontological studies as well as for oxygen and carbon isotope analyses, and (2) because clastic sedimentation in the region strongly depends on ice-rafting controlled by water currents and climate. As a result of previous studies, several hypotheses have been presented about ocean circulation changes between the "warm" and "cold" periods of Late Pleistocene–Holocene time. The general idea is that the pattern of surface water currents did not vary significantly (Kent et al., 1971; Sancetta, 1983), whereas changes of intermediate water currents may have been important (Duplessy et al., 1988). Less is known about the history of deep-ocean circulation. Broecker et al. (1985) and Broecker and Denton (1989) proposed two modes of ocean circulation: (1) with the North Atlantic source of deep water running in post-glacial and interglacial periods; and (2) with the North Pacific source of deep water becoming significant in glacial time. However, that scenario is not supported by the available carbon isotopic evidence from benthic foraminifera (Keigwin, 1987; Keigwin et al., 1992).

The purpose of the work reported is to find the main provenances and pathways of the fine- and medium-grained clastics contained in the glacial and interglacial sediments of the northwest Pacific

0025-3227/94/$7.00
SSDI 0025-3227(93)E0108-I

and to use these to check the various hypotheses about ocean circulation change. Our previous study of heavy mineral assemblages in the central Pacific as indicators of provenance (Nechaev, 1991) proved to be very helpful in this research.

For the present study, 97 samples of Quaternary sediments were obtained by gravity and box coring in the northwest Pacific Ocean (including the Kuril and Aleutian Trenches and the Bering Sea) during Leg 19/4 of the Russian R/V *Akademik Aleksandr Vinogradov* cruise in July 1991 (Table 1; Fig. 1). The data from other North Pacific areas were compiled from previously published work (Petelin, 1957; Aleksina, 1962; Lisitsyn, 1966; Griggs and Kulm, 1969; Conolly and Ewing, 1970; Kent et al., 1971; Scheidegger et al., 1973; McManus et al., 1977; Nechaev, 1991). In addition, we studied the mineralogy of 11 samples from the Vancouver Island area (Canada) obtained from Dr J. Vaugh Barrie and Trudie C. Forbes of the Geological Survey of Canada.

2. Methods

For the mineral analyses, the 0.05–0.1 mm fraction was separated from the sediment samples by wet sieving. After bulk mineral analysis of this fraction (carried out by A.V.S.) (Table 2), heavy minerals were extracted using tribromomethane (density 2.89), and analyses were conducted by V.P.N. (Table 3). All the minerals were identified using a petrographic microscope, Canadian balsam and, when necessary, immersion oils.

A stratigraphic study based on diatoms was performed by I.B.T. The glacial and interglacial stages of the Late Pleistocene and Holocene were identified by the relative abundance of selected diatoms: (1) *Neodenticula seminae* prevailing in the post- and interglacial periods; and (2) *Thalassiosira latimarginata–Actinocyclus curvatulus* Group and *Thalassiosira* species dominating in the glacial epochs (Baldauf, 1982; Sancetta, 1983; Sancetta and Robinson, 1983; Sancetta and Silvestri, 1984). For age determination of the older sediments, the North Pacific Diatom Zonation proposed by Akiba (1986) was used. In some instances the Holocene/Late Pleistocene boundary was interpreted on the basis of the sedimentation rates known from previous investigations in the region (Creager et al., 1973; Morley et al., 1982; Keigwin, 1987; Gorbarenko, 1991; Sancetta and Robinson, 1983; Keigwin et al., 1992).

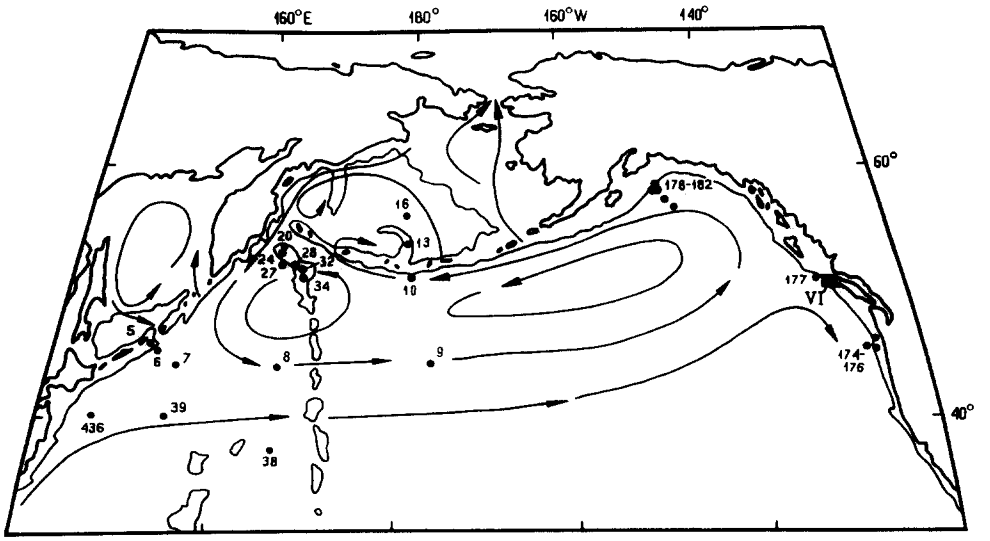

Fig. 1. Sample locations and scheme of modern surface water currents in the subarctic North Pacific (after Dodiemead et al., 1963; Arsen'ev, 1967; Yasuoka, 1967; 1968). *VI* = the studied area off Vancouver Island. Data on the DSDP Sites (174–182 and 436) were compiled from previously published work (Scheidegger et al., 1973; Nechaev, 1991).

Table 1
List of samples

Station	Latitude–Longitude	Water depth (m)	Setting	Lithology
Kuril Trench				
GC5	46°00.2'N–150°42.9'E	2110	Island slope	0–5 cm: sand, dark gray, with single gravel
GC6	45°31.8'N–152°15.5'E	5500	Island slope	0–60 cm: silty clay, siliceous, dusky yellowish brown in 0–12 cm and grayish olive green below
Hokkaido Rise				
GC7	45°00.1'N–154°59.0'E	4990	Flat seafloor	0–73 cm: silty clay, siliceous, dark brown in 0–43 cm and light olive below
Northwest Pacific Basin				
BC8	44°57.7'N–165°06.4'E	5860	Flat seafloor	0–60 cm: silty clay, siliceous with sand and gravel on the surface, brown in 0–58 cm and light olive gray below
North Pacific Basin				
GC9	44°36.3'N–176°49.4'W	6100	Flat seafloor	0–255 cm: silty clay, siliceous, brown, with pumice pebbles covered by Mn crust at 15,12 and 20 cm. There is volcanic ash in 208–210 cm
Aleutian Trench				
GC10	50°53.6'N–178°56.2'W	4000	Island slope	0–170 cm: clayey silt, dark yellowish brown in upper 3 cm and olive gray below, with thin lenses and layer (54–55 cm) of volcaniclastic sand
Bowers Ridge, Bering Sea				
GC13	53°41.1'N–178°43.0'E	2630	NE slope	0–5 cm: silty clay, siliceous, grayish brown 5–93 cm: silty and sandy clay, siliceous and calcareous, dusky yellow green in the upper part and grayish olive green below 93–95 cm: clayey sand, calcareous, grayish black 95–520 cm: sandy and silty clay, calcareous and siliceous, grayish olive green in 93–105, 106.5–117, 150–520 cm and dusky yellow green in other intervals 520–620 cm: sandy clay calcareous, dusky yellow green
Aleutian Basin, Bering Sea				
BC16	56°00.2'N–179°59.0'E	3815	Flat seafloor	0–60 cm: silty clay, siliceous, moderate brown in 0–22 cm and grayish olive below
Meiji Seamount				
GC20	53°35.6'N–164°49.3'E	3430	NE slope	0–62 cm: sandy and silty clay, moderate brown on the top and light olive gray below
GC24	52°58.2'N–164°43.1'E	2970	Flat top	0–33 cm: sandy clay, calcareous: dark yellowish brown in 0–18 cm, light olive brown in 18–20 cm, moderate brown in 21–23 cm, light olive gray in 23–28 cm, moderate olive brown in 28–33 cm. There are ash layers: brown in 20–21 cm and light gray at 23 cm (3 mm in thickness). 33–94 cm: silty clay, siliceous grayish olive green
Basin between Meiji and Detroit Seamounts				
BC27	51°23.0'N–165°04.7'E	5120	Flat seafloor	0–39 cm: sandy and silty clay, siliceous: dark yellowish brown in 0–17 cm, pale brown in 18–21 cm, grayish brown in 23.5–34 cm, dusky brown in 34–39 cm. There are ash layers: dusky yellowish brown in 17–18 cm and light gray in 21–23.5 cm 39–53 cm: silty clay, olive gray

Table 1 (*continued*)

Station	Latitude–Longitude	Water depth (m)	Setting	Lithology
Detroit Seamount				
GC28	51°18.0'N–167°39.9'E	2340	Flat top	0–22 cm: foram sand, clayey: dark yellowish brown in 0–5 cm and light olive gray in 5–22 cm. There are ash lenses yellowish gray at 7 cm 22–39 cm: sandy clay, calcareous grayish olive, with pale olive spots, bioturbated 39–450 cm: Silty and sandy clay: olive gray in 39–282 cm, grayish olive green in 303–317 cm, dusky yellow green in 320–335, 350–370 and 378–450 cm, dark greenish gray in 335–350 and 370–378. There are ash layers: brownish black in 170–180 cm (1 cm in thickness, oblique to the core axis) and light olive gray in 317–320 cm
GC32	51°03.4'N–167°52.8'E	2860	Southern slope	0–19 cm: foram sand, clayey: dark yellowish brown in 0–12 cm and light olive in 12–19 cm 19–35 cm: sandy clay, calcareous, light olive gray, with light olive brown and grayish olive spots, bioturbated 35–575 cm: sandy and silty clay: olive gray in 35–320 and 360–380 cm, dusky yellow green in 320–345 cm and grayish olive green in 345–360 cm and 380–575 cm. There are ash layers: brownish black at 193 cm (7 mm in thickness), moderate brown in 517–520 cm and 545–575 cm (1–3 cm in thickness — core in this section is disturbed)
GC34	50°36.3'N–168°07.8'E	3750		0–14 cm: sandy clay, calcareous, moderate brown 14–620 cm: silty and sandy clay: light olive gray in 14–60 cm, olive gray in 60–337 cm and grayish olive in 337–620 cm. There are ash layers: light olive gray at 98 and 360 cm and grayish brown at 578 cm (0.5 cm in thickness)
Northwest Pacific Basin				
BC38	38°04.7'N–165°11.1'E	5370	Flat seafloor	0–65 cm: clay, moderate brown in 0–20 cm and pale olive in 20–65 cm
GC39	40°00.0'N–153°29.2'E	5620	Flat seafloor	0–196 cm: silty clay, siliceous: moderate brown in 0–24 cm, light olive gray in 24–63 cm, grayish olive green in 63–196 cm. There are ash layers yellowish gray in 85–86 and 178–181 cm
Vancouver Island area				
PAN77-11	50°20.7'N–128°09.2'E	137	Shelf	Muddy fine sand, olive gray
PAN77-25	50°16.4'N–128°03.7'E	71	Shelf	Gravelly sand, olive gray
PAN77-86	50°42.0'N–128°36.7'E	141	Shelf	Muddy fine sand, olive gray
PAN77-107B	50°41.9'N–128°44.5'E	170	Shelf	Muddy fine sand, olive gray
PAN78-44	50°50.6'N–129°15.3'E	113	Shelf	Speckled foram/volcaniclastic sand
PAN78-56	50°55.1'N–129°21.5'E	170	Shelf	Muddy fine foram sand, olive gray
PAN78-59	50°51.3'N–129°25.1'E	183	Shelf	Muddy medium foram sand, green
PAN76-93	50°51.3'N–129°25.1'E	104	Shelf	Muddy fine sand, olive gray, with pebble
PAR86a-018	51°27.0'N–128°22.5'E 51°26.9'N–128°22.2'E	130–122	Shelf	Sandy mud, green, with boulder and gravel
PAR86a-024	51°27.7'N–128°35.0'E	143	Shelf	Silty sand, dark, slightly greenish
End78-003	50°02.2'N–127°43.1'E	80	Shelf	Shelly and pebbly fine sand, dark olive gray

GC = Gravity corer; BC = box corer. Samples from the Vancouver Island area have been obtained by grab sampler, excluding PAR86a-018 which was obtained by dredging.

Table 2
Percentages of minerals in the 0.05–0.1 mm fraction of the North Pacific sediments

Site (interval in cm)	Q	Fsp1	Fsp2	L	Bi	Mus	Chl	HV	Op	Gl1	Gl2	Gl3	Dt	Rd	Frm	Cc	No.
GC5	—	32.4	3.3	—	—	—	—	28.3	23.5	6.3	1.1	2.6	—	0.7	1.8	—	272
GC6, 0–12	—	24.5	5.0	—	—	0.4	—	4.7	23.4	18.0	20.5	—	1.4	2.2	—	—	278
12–25	0.4	27.1	3.2	—	—	—	—	4.6	11.7	6.1	19.8	3.0	15.9	7.2	1.1	—	571
25–50	0.4	23.8	0.6	—	—	—	—	3.5	18.4	6.8	13.5	1.2	19.7	11.9	—	0.2	488
GC7, 0–15	0.2	19.6	0.7	—	—	—	—	4.0	21.2	2.6	16.5	0.2	28.3	6.6	—	—	424
15–40	0.8	24.1	5.7	—	1.1	—	—	8.1	20.6	4.1	21.0	—	13.6	1.1	—	—	369
40–73	—	20.6	2.1	—	—	—	—	4.5	10.4	—	50.7	0.6	5.1	6.0	—	—	335
BC8, 0–35	0.2	29.7	1.5	—	3.2	—	0.2	5.0	12.9	2.2	28.5	—	9.9	6.7	—	—	403
35–40	—	38.7	3.0	—	8.3	1.3	—	5.7	14.7	4.0	16.3	—	4.3	3.7	—	—	300
40–60	—	39.7	10.5	—	1.1	—	—	4.6	18.1	1.1	15.1	0.3	3.5	5.9	—	—	370
GC9, 0–23	—	12.9	3.6	—	—	—	0.3	2.8	5.8	1.1	13.2	—	28.7	31.7	—	—	363
23–100	—	14.1	1.0	—	3.3	—	—	3.3	5.2	2.3	38.4	—	16.7	15.7	—	—	305
100–208	—	20.8	2.6	—	7.8	—	—	5.2	10.1	7.8	22.5	—	9.4	13.7	—	—	307
208–210	—	13.0	—	—	1.3	—	—	1.8	12.8	23.6	29.7	0.2	11.0	6.1	—	0.5	555
210–250	—	8.9	1.4	—	—	—	—	0.7	6.3	4.0	15.6	0.2	21.9	41.0	—	—	429
GC10, 0–15	—	27.1	1.4	—	0.3	—	—	10.5	17.6	10.8	3.4	—	8.8	20.0	—	—	295
15–50	—	16.7	3.4	—	3.2	0.3	—	9.9	12.8	9.9	2.3	—	13.8	27.6	—	—	384
55–100	—	21.5	4.0	—	5.8	—	0.6	10.1	17.8	16.6	3.1	—	8.9	11.6	—	—	326
100–165	—	35.7	5.8	—	1.1	—	0.4	12.6	22.4	18.8	2.2	—	0.4	0.7	—	—	277
GC13, 0–5	—	8.1	2.1	—	4.4	—	—	4.7	30.2	9.4	3.9	—	32.0	5.2	—	—	384
5–93	—	9.0	0.2	—	—	—	—	1.5	3.8	6.5	1.9	—	48.3	21.5	6.1	1.0	522
93–117	—	25.1	3.4	—	4.1	—	—	3.2	10.7	13.9	1.6	0.7	5.5	2.3	29.0	0.4	438
117–150	—	25.4	1.1	—	4.5	—	—	4.2	7.9	2.8	4.2	—	11.6	4.5	33.6	—	354
150–268	1.0	43.8	6.6	—	12.5	—	0.3	3.9	21.7	4.6	2.3	—	0.7	0.6	1.3	0.7	304
268–350	2.7	42.7	3.5	—	9.4	—	1.4	9.8	16.4	2.4	0.7	—	6.6	1.4	2.1	0.7	286
350–435	0.4	39.9	10.0	—	5.8	—	0.4	9.3	13.7	6.3	1.8	—	7.0	2.9	2.0	0.4	446
435–520	1.5	18.8	7.9	—	3.2	—	—	3.2	10.6	4.1	0.9	—	27.9	19.1	2.6	0.3	341
520–620	4.9	30.1	4.5	—	7.9	—	—	9.7	13.2	4.5	2.1	—	11.3	8.2	3.7	—	380
BC16, 0–25	0.2	6.3	2.9	—	—	—	—	0.7	3.4	3.8	—	—	74.5	8.2	—	—	416
25–60	1.5	3.0	1.2	—	0.9	1.2	—	2.1	1.2	1.2	1.2	0.3	77.8	8.2	—	—	329
GC20, 0–10	—	33.3	6.3	—	—	—	—	13.6	17.1	6.8	13.6	—	6.0	2.9	0.3	—	381
20–40	3.8	37.3	5.7	—	9.4	—	1.9	8.5	18.9	8.0	4.2	—	1.4	—	0.5	0.5	212
40–50	2.4	26.7	16.7	—	13.4	—	0.3	3.6	21.4	3.0	7.1	—	3.0	2.4	—	—	336
GC24, 0–10	0.8	25.5	1.0	—	—	—	—	9.6	14.4	4.5	11.1	—	12.6	2.8	17.7	—	396
10–18	0.5	16.7	1.0	—	—	—	—	7.6	15.4	1.8	16.7	—	16.2	1.1	23.0	—	383
18–20 (ash)	1.2	13.5	3.5	—	2.3	—	—	6.9	5.0	—	6.2	—	44.4	0.4	16.6	—	259
20–21 (ash)	—	8.4	3.0	—	—	—	—	1.0	9.1	1.3	77.0	—	0.3	—	—	—	395
21–23	—	17.1	5.3	—	1.4	—	0.6	7.0	14.9	2.2	49.7	—	0.3	0.3	0.6	0.6	356
23 (ash)	0.7	20.5	0.3	—	4.8	—	—	5.1	11.9	—	43.7	—	6.8	—	6.1	—	293
23–33	—	14.8	2.3	—	3.7	—	0.2	5.1	9.2	1.2	50.8	—	3.0	—	9.7	0.0	433
35–55	4.5	39.6	5.2	—	6.3	—	0.4	10.5	16.8	—	12.3	—	3.5	—	0.7	—	285
55–90	6.1	47.0	7.9	—	3.6	—	0.8	11.1	13.3	2.9	3.6	—	2.5	1.1	—	0.4	279
BC27, 0–12	0.2	20.2	0.8	—	1.5	—	—	4.5	21.1	2.0	30.4	—	16.6	3.0	—	—	559
12–17	0.3	24.3	2.6	—	3.9	—	—	9.9	7.1	1.0	32.2	—	17.3	1.3	—	—	382
17–18 (ash)	—	34.8	6.0	—	1.8	—	—	12.4	12.1	1.1	26.6	—	4.6	0.7	—	—	282
18–21	—	17.1	3.8	—	0.6	—	—	3.8	4.8	0.6	60.6	—	8.6	—	—	—	315
21–23.5 (ash)	—	15.6	3.3	—	0.3	—	—	2.4	4.2	2.1	65.2	—	6.6	0.3	—	—	333
23.5–34	—	10.6	3.8	—	2.1	—	—	1.7	5.2	0.5	5.7	—	63.9	6.6	—	—	424
34–39	—	13.3	5.0	—	3.0	0.5	—	1.5	5.8	0.3	2.0	—	53.8	14.9	—	—	398
39–42	—	6.5	2.0	—	—	—	—	0.8	5.4	0.6	1.7	—	61.1	22.0	—	—	355
42–53	—	40.7	8.3	—	6.7	—	1.3	10.2	9.3	—	4.8	—	17.6	0.9	—	0.3	312

Table 2 (*continued*)

Site (interval in cm)	Q	Fsp1	Fsp2	L	Bi	Mus	Chl	HV	Op	Gl1	Gl2	Gl3	Dt	Rd	Frm	Cc	No.
GC28, 0–22	—	10.8	0.2	—	0.6	—	—	1.9	4.4	0.6	9.4	—	29.9	15.0	27.2	—	519
22–39	—	6.1	—	—	0.9	0.2	—	1.4	—	—	1.2	—	45.7	10.1	34.4	—	427
39–116	1.0	22.7	5.2	—	14.1	—	—	7.3	7.3	1.0	5.7	—	17.0	6.0	13.6	—	383
116–170	—	23.9	—	—	6.3	—	—	2.5	7.7	1.8	38.8	—	9.7	3.9	5.4	—	443
170–180 (ash)	—	12.8	2.3	—	0.9	—	—	4.8	8.7	3.2	64.4	—	0.4	0.2	2.1	—	436
170–227	—	8.6	—	—	1.7	—	—	1.3	5.8	1.5	26.5	—	31.6	6.3	16.8	—	465
227–282	—	39.3	7.3	—	4.8	—	—	9.0	14.3	5.3	2.4	—	10.4	3.6	3.4	—	412
282–303	—	9.2	—	—	0.3	—	—	1.9	2.2	—	14.3	—	66.0	6.0	—	—	315
303–317	—	18.8	4.1	—	1.5	—	—	3.8	5.3	1.3	37.2	—	24.7	3.4	—	—	320
317–320 (ash)	—	1.4	1.4	—	—	—	—	0.7	5.2	—	89.9	—	1.4	—	—	—	287
320–335	—	12.2	0.9	—	0.2	—	—	3.3	3.5	1.4	16.4	—	52.9	4.4	4.4	0.2	427
335–350	—	10.6	1.5	—	0.7	—	—	4.0	5.3	4.0	15.0	—	40.3	14.9	3.5	—	451
350–370	—	13.5	1.3	—	1.5	—	—	3.1	0.5	1.8	23.7	—	20.7	2.1	31.9	—	392
370–378	—	17.8	4.6	—	1.6	—	—	6.3	6.3	—	46.4	—	13.4	1.3	1.6	0.5	366
378–450	—	5.0	0.5	—	0.5	—	—	0.5	2.4	0.8	9.7	—	57.6	22.0	1.0	—	382
GC32, 0–19	—	11.0	—	—	0.2	0.2	—	3.0	2.8	0.6	19.7	—	28.9	3.4	30.1	0.2	529
19–35	—	4.7	0.4	—	—	—	—	0.2	—	—	5.1	—	54.8	9.5	25.2	0.2	531
35–185	3.3	37.3	6.9	—	1.3	—	—	7.6	12.5	2.0	14.7	—	9.4	3.1	2.0	—	394
185–320	4.1	28.5	1.9	—	5.6	—	—	5.9	11.1	—	6.7	—	26.3	4.1	5.6	—	270
320–345	—	5.4	—	—	2.3	—	—	1.1	0.5	2.3	5.7	—	73.0	9.5	0.2	—	441
345–360	—	19.1	—	—	4.1	0.6	—	2.4	2.4	1.5	59.9	—	9.7	0.2	—	0.2	466
360–380	—	12.2	—	—	1.6	0.5	—	1.6	1.6	1.8	40.6	—	32.3	7.5	0.3	—	384
380–441	—	16.8	—	—	4.4	—	—	3.3	3.0	3.6	18.7	—	36.3	7.7	6.0	0.3	364
441–517	—	19.3	—	—	4.4	—	—	3.9	3.1	2.7	31.5	—	25.1	7.2	2.7	—	517
517–520 (ash)	—	14.9	—	—	1.2	—	—	1.2	4.4	6.1	71.1	—	1.2	—	—	—	343
520–575	—	8.6	—	—	1.0	0.3	—	1.6	3.2	1.0	76.8	—	6.0	1.6	—	—	315
GC34, 0–14	—	21.8	2.0	—	0.6	—	—	8.8	6.5	0.8	15.7	1.0	16.5	4.5	21.6	—	490
14–60	0.3	40.0	2.9	—	20.3	—	—	16.4	11.0	1.3	1.6	—	4.2	1.3	1.0	—	310
60–98	—	38.9	—	—	16.4	—	—	4.5	10.3	5.0	18.3	—	3.4	3.1	—	—	262
98–100	—	16.1	—	—	1.5	—	—	6.2	7.6	5.9	61.3	0.6	0.9	—	—	—	341
100–200	—	25.4	1.0	—	7.0	—	0.3	3.5	8.7	3.1	29.6	—	20.2	1.0	—	—	287
200–260	—	37.7	3.2	—	9.2	—	0.5	6.7	7.8	4.3	21.3	—	5.4	3.7	—	—	371
260–337	—	23.0	2.7	—	11.0	0.3	—	6.0	17.8	3.0	22.1	—	10.9	3.0	0.3	—	366
337–420	—	28.0	0.5	—	19.3	0.3	—	7.3	7.8	1.3	29.8	—	5.4	0.3	—	—	372
360 (ash)	—	17.6	—	—	15.5	3.0	—	2.7	3.3	3.3	20.2	—	28.9	5.7	—	—	336
420–578	—	24.7	—	—	8.7	0.3	—	1.0	8.5	3.9	35.0	—	16.5	1.6	—	—	389
578 (ash)	—	3.1	0.5	—	1.6	—	—	2.6	0.5	—	91.6	—	—	—	—	—	382
578–620	—	14.7	0.5	—	17.6	0.8	—	2.4	4.0	2.4	42.4	—	6.1	9.1	—	—	375
BC38, 0–15	—	0.2	—	—	—	—	—	—	0.4	—	1.5	—	20.2	77.6	—	—	461
15–30	—	—	—	—	—	—	—	0.2	2.3	0.9	1.1	—	52.9	42.8	—	—	435
30–65	—	0.7	—	—	1.5	0.2	0.2	—	0.5	—	4.7	—	3.5	87.1	1.5	—	405
GC39, 0–24	—	9.7	—	—	3.7	—	—	1.9	4.7	1.0	19.4	—	27.5	32.1	—	—	516
24–85	—	11.7	—	—	7.9	—	—	2.2	8.2	1.4	41.3	—	8.5	18.9	—	—	366
85–86	—	24.2	—	—	1.3	—	—	6.7	6.5	—	61.3	—	—	—	—	—	372
86–196	—	9.3	—	—	3.6	—	—	1.7	4.4	0.4	12.9	—	49.8	17.8	—	—	472
178–181	—	6.8	—	—	2.2	—	—	1.5	1.8	2.2	84.0	—	0.9	0.6	—	—	325
Vancouver Island area																	
PAN77-11	26.3	1.6	8.2	51.9	—	0.3	1.3	7.3	3.2	—	—	—	—	—	—	—	316
PAN77-25	20.8	0.6	8.5	57.4	—	0.6	—	4.8	3.0	—	0.6	—	—	0.3	0.6	2.7	331
PAN77-86	15.2	1.0	7.6	38.1	—	0.3	—	23.8	13.3	—	—	—	—	—	0.3	0.3	315
PAN77-107B	18.4	0.9	4.7	40.5	—	—	—	19.3	14.6	—	—	—	—	0.3	—	1.3	316
PAN78-44	16.1	—	5.5	38.0	—	0.6	—	4.9	6.4	—	—	—	—	0.3	1.5	26.7	329

Table 2 (*continued*)

Site (interval in cm)	Q	Fsp1	Fsp2	L	Bi	Mus	Chl	HV	Op	Gl1	Gl2	Gl3	Dt	Rd	Frm	Cc	No.
PAN78-56	18.5	2.3	10.0	36.1	—	0.3	—	19.9	11.1	—	—	—	—	—	0.3	1.5	341
PAN78-59	21.0	2.5	14.9	47.3	—	1.0	—	6.0	2.5	—	—	—	—	0.3	0.3	4.1	315
PAR76-93	8.3	2.1	8.6	24.2	—	0.3	—	15.9	38.1	—	—	—	—	—	0.6	2.1	339
PAR86a-18	41.8	0.6	20.9	20.6	—	—	—	9.3	3.3	—	—	—	—	0.6	—	3.0	335
PAR86a-24	34.3	3.4	20.5	20.8	—	—	0.6	13.8	4.0	—	—	—	—	—	0.6	2.1	327
End78-3	14.7	—	23.2	48.6	—	1.5	0.3	8.0	3.4	—	—	—	—	—	—	0.3	327

Q = quartz; Fsp = feldspar (1 = fresh, 2 = altered); L = lithoclasts; Bi = biotite; Mus = muscovite, Chl = chlorite, HV = transparent heavy minerals; Op = opaque minerals; Gl = volcanic glass (1 = brown, 2 = colourless, 3 = altered); Dt = diatom; Rd = radiolaria; Fm = foraminifera; Cc = irregular calcite grains; No. = number of grains counted; dashes = not found.

3. Age of the sampled sediments

The oldest sediments were recovered at Site 9 (Table 1; Figs. 1 and 5) in the central North Pacific Basin where the samples of interval 170–255 cm represents the *Actinocyclus oculatus* Zone of the Early Pleistocene. In the upper core sections, the *Rhizosolenia curvirostus* Zone of the Middle Pleistocene (125–170 cm) and the *Neodenticula seminae* Zone of the Late Pleistocene (0–125 cm) were defined. The Holocene sediments are suggested to be in the 0–25 cm interval of this core because *Nitzchia* species are essentially absent here. Samples from all the other cores obtained during the *Vinogradov* Leg 19/4 cruise contain only the Late Pleistocene–Holocene diatom assemblages.

In the central Northwest Pacific Basin (Sites 7, 8, 38 and 39; see Fig. 1), the rates of sedimentation are 3–5 cm/kyr (Morley et al., 1982), hence, the Holocene sediments are expected in the upper 30–50 cm of these cores (Figs. 4, 10 and 11). Only sediments of Site 8 have been used in our biostratigraphic study (Fig. 4). As a result, the Holocene clay with abundant *Neodenticula seminae* was found in the interval 0–35 cm of this core. Below this (35–60 cm), the Late Wisconsin sediments containing the increasing *Thalassiosira trifulta–Actinocyclus curvatulus* Group and some displaced shelf species were defined.

In the well-studied area of the northern Emperor Seamounts (Meiji and Detroit, Sites 20, 24, 27, 28, 32 and 34; see Fig 1), the sedimentation rates are at least 3–5 cm/kyr (Creager et al., 1973; Keigwin, 1987; Gorbarenko, 1991; Keigwin et al., 1992). Only our paleontological data obtained for Site 24 (Meiji Guyot) support this definition. The Holocene-Pleistocene boundary was found at 31 cm in this core (Fig. 8).

In the Kuril and Aleutian Trenches, the known rates of sedimentation are more than 10 cm/kyr (Creager et al., 1973; Morley et al., 1982). The diatom fossil assemblages in all the sediments sampled at Sites 5 and 6 (Kuril Trench) are homogeneous with *Neodenticula seminae* dominating to at least 60 cm downcore. This, together with the preceding observation, suggests their Holocene age. At Site 10 (Aleutian Trench) the corer reached Late Pleistocene sediments (not deeper), and the Pleistocene–Holocene boundary is placed at 90 cm (Fig. 6). The diatom complex throughout the core is markedly contaminated by benthic and Paleogene–Neogene species.

The sedimentation rates in the central and southern Bering Sea where Sites 13 and 16 are located (Fig. 1), are more than 13 cm/kyr (Sancetta and Robinson, 1983). We did not examine biofossils in these cores. However, during the *Vinogradov* Leg 19/4 cruise we obtained another core from this area (Site 11 located at 53°31'N–178°51'E on the Bowers Ridge) and the diatom assemblages were studied. Site 11 has 161 cm of Holocene, about 450 cm of Late Wisconsin and 150 cm of Middle Wisconsin clays (their mineralogy was not studied). The lithological sequence in the core from Site 13 is fairly similar to that from the nearby Site 11. Sediments from Site 13 (0–620 cm) are therefore presumed to be of the same or similar

Table 3
Percentage of heavy clastic minerals in the 0.05–0.1 mm fraction of the North Pacific sediments

Site, interval in cm	Ol	Id	Cpx1	Cpx2	Opx	Hb	Am	Ep	Gm	Zr	Trm	St	Mon	Ap	Sph	Rt	Bi	Op	No.
GC5	1.8	—	1.3	41.4	14.7	2.8	0.3	5.9	—	—	—	—	—	1.3	0.5	—	—	30.1	389
GC6, 0–12	0.6	—	0.9	55.1	17.8	1.8	0.3	4.8	—	—	—	—	—	0.6	—	—	—	18.1	332
12–25	1.3	—	—	50.0	17.1	2.3	0.3	5.8	—	—	—	—	—	0.6	—	—	0.3	22.3	310
25–50	—	0.3	0.3	50.6	19.1	4.1	1.3	5.3	—	—	—	—	—	0.3	—	—	—	18.8	320
GC7, 0–15	1.6	0.3	0.3	44.9	5.4	2.6	0.3	9.0	—	—	—	—	—	1.0	—	—	—	34.6	312
15–40	—	—	0.7	47.0	7.9	11.8	0.3	10.2	—	—	—	—	—	0.3	—	—	—	21.7	304
40–73	—	—	—	37.6	10.2	14.3	1.3	7.0	—	—	—	—	—	0.6	—	—	0.3	28.7	314
BC8, 0–35	—	—	—	14.3	6.1	0.5	0.3	9.3	0.3	—	—	—	—	0.5	—	—	—	68.7	377
35–40	0.3	—	—	24.2	6.2	2.5	1.9	11.5	0.3	—	—	—	—	0.6	—	—	—	52.5	322
40–60	—	—	—	17.9	8.8	2.8	3.5	7.2	—	—	—	—	—	1.6	—	—	—	58.2	318
GC9, 0–23	—	0.3	—	19.3	5.3	4.4	4.7	10.6	0.3	—	—	—	—	0.3	—	—	—	54.8	321
23–100	—	—	—	12.5	3.4	1.6	3.4	9.7	0.6	0.6	—	—	—	0.3	—	—	—	67.8	320
100–208	—	—	—	17.4	3.7	4.4	2.5	17.8	—	0.3	—	—	—	0.3	—	—	—	53.6	321
208–210	—	—	—	33.4	17.5	1.0	—	1.3	—	—	—	—	—	1.0	—	—	—	45.9	314
210–250	—	—	0.3	24.4	9.4	3.1	4.1	13.4	0.6	0.3	—	0.3	—	0.3	—	—	—	43.8	320
GC10, 0–15	0.3	—	—	39.0	8.7	1.6	0.3	9.5	—	0.3	—	—	—	0.3	—	—	—	40.1	367
15–50	—	—	—	36.3	2.4	1.7	0.6	3.0	—	—	—	—	—	—	—	—	—	55.9	465
55–100	—	—	0.3	40.4	6.4	10.2	2.5	23.2	—	—	—	—	—	0.6	—	—	—	16.2	314
100–165	—	—	—	44.2	4.2	17.3	1.4	4.8	—	—	—	—	—	0.3	—	—	—	27.8	353
GC13, 0–5	2.6	—	—	50.8	8.9	5.9	1.0	9.5	—	—	—	—	—	0.7	—	—	—	20.7	305
5–93	1.2	—	—	38.2	6.5	2.5	0.3	6.5	0.3	—	—	—	—	1.2	0.3	—	—	43.1	325
93–117	—	—	—	25.3	3.7	4.6	8.2	18.3	1.5	0.6	—	—	—	1.2	—	—	—	36.6	328
117–150	—	—	—	36.7	10.5	5.4	5.1	11.5	—	0.3	—	—	—	1.0	—	—	0.3	29.1	313
150–268	—	—	1.9	14.4	4.5	7.0	11.8	31.9	4.2	0.6	—	—	—	2.6	1.0	—	—	20.1	313
268–350	—	—	1.6	19.4	3.8	9.5	13.7	23.2	4.4	0.3	—	—	—	1.0	0.6	—	—	22.5	315
350–435	—	—	—	21.1	4.5	14.8	9.7	27.8	3.3	1.2	0.6	—	—	2.1	0.3	—	—	14.5	331
435–520	—	—	0.6	16.8	5.5	10.1	7.0	35.8	2.8	—	1.2	—	—	2.1	0.3	0.6	—	17.1	327
520–620	—	—	0.3	14.0	6.5	5.8	7.1	26.3	3.2	0.3	0.3	—	0.3	0.6	0.3	—	—	34.7	308
BC16, 0–25	0.3	—	0.3	21.1	5.0	8.5	14.8	26.1	1.3	0.3	0.3	—	0.6	1.3	0.3	—	—	19.8	318
25–60	—	0.6	0.3	10.8	3.8	15.6	9.9	23.9	2.9	—	0.3	—	—	1.3	0.3	—	—	30.3	314
GC20, 0–10	0.3	—	0.6	18.3	9.9	16.7	2.2	6.4	0.3	—	—	—	—	0.6	0.6	—	—	43.9	312
20–40	—	—	0.2	25.7	18.0	17.5	4.9	11.4	1.2	0.2	—	—	—	0.7	—	—	—	20.1	412
40–50	0.6	—	1.3	19.2	4.7	15.8	3.8	19.2	1.9	0.6	—	—	0.3	1.3	0.3	—	—	30.9	317
GC24, 0–10	—	—	1.3	20.8	15.0	22.5	0.3	6.8	—	—	0.3	—	—	—	—	—	—	32.9	307
10–18	—	—	0.6	24.9	14.4	21.1	0.6	1.3	—	—	—	—	—	—	—	—	—	37.1	313
18–20 (ash)	—	—	0.6	11.9	5.5	42.3	0.6	5.8	0.3	—	—	—	—	0.3	—	—	—	32.6	310
20–21 (ash)	0.3	—	—	25.3	16.4	0.9	0.3	0.9	0.0	—	—	—	—	0.9	—	—	0.3	54.6	324
21–23	—	0.3	—	22.3	9.8	0.7	—	2.6	0.0	—	—	—	—	—	—	—	—	64.3	305
23 (ash)	—	—	—	22.9	21.6	4.5	—	—	0.0	—	—	—	—	—	—	—	—	51.0	310
23–33	—	—	—	21.5	11.8	3.9	0.6	3.0	0.0	—	—	—	0.3	0.6	—	—	—	58.2	330

35–55	—	—	—	21.8	23.0	7.6	4.8	8.8	0.3	—	—	—	—	—	—	—	—	33.8	331
55–90	—	—	—	19.0	10.6	13.7	5.9	16.8	1.2	0.3	—	—	0.3	0.3	—	—	0.3	31.5	321
BC27, 0–12	—	—	0.3	29.6	12.5	2.1	0.9	2.7	0.0	—	—	—	—	0.9	—	—	—	51.0	335
12–17	—	—	—	23.2	12.5	1.9	0.6	5.8	0.3	—	—	—	—	0.3	0.3	—	—	55.0	311
17–18 (ash)	—	—	—	29.4	19.7	1.3	0.3	5.2	0.0	—	—	—	—	—	—	—	0.3	43.9	310
18–21	—	—	—	20.9	13.4	0.7	0.3	4.2	1.0	—	—	—	—	—	—	—	—	59.5	306
21–23.5 (ash)	0.3	—	—	15.5	15.1	0.3	—	1.9	0.0	—	—	—	—	0.3	—	—	—	66.6	317
23.5–34	—	—	—	9.0	6.5	1.9	1.6	8.4	0.9	—	—	—	—	0.3	—	—	—	71.3	321
34–39	—	—	0.6	12.3	7.6	2.5	1.6	16.8	2.8	—	—	—	—	0.3	—	0.3	—	55.1	316
39–42	—	—	0.6	13.2	7.4	5.2	3.4	23.4	2.8	—	—	0.6	—	1.2	0.3	0.3	—	41.5	325
42–53	—	—	—	12.5	6.6	11.6	6.9	25.4	2.5	0.3	—	—	—	0.9	0.3	—	—	32.9	319
GC28, 0–22	—	—	—	13.4	11.3	3.3	0.3	4.2	0.0	—	—	—	—	0.3	—	—	—	67.3	336
22–39	0.3	—	—	12.2	6.1	4.1	3.5	28.3	5.8	0.3	—	—	—	1.2	0.6	0.3	—	37.3	343
39–116	—	—	0.3	16.2	8.3	10.1	8.6	19.3	2.8	0.3	1.2	—	—	1.2	0.6	—	—	31.2	327
116–170	0.3	—	—	11.5	9.3	3.5	3.5	15.7	0.0	0.3	—	—	—	0.6	—	—	—	55.1	312
170–180 (ash)	—	—	—	41.8	15.2	0.3	—	1.8	0.3	—	—	—	—	—	—	—	—	40.6	330
170–227	—	—	—	11.3	9.5	1.8	—	6.7	0.6	—	—	—	—	0.9	—	—	—	69.1	327
227–282	—	—	—	16.0	10.6	6.2	5.0	21.8	2.0	0.3	—	—	0.3	0.3	—	—	—	37.5	357
282–303	—	—	—	14.6	5.6	3.1	3.4	14.9	2.8	0.6	—	—	—	0.3	—	0.3	—	54.5	323
303–317	—	—	1.3	14.4	6.3	5.0	5.6	16.9	1.6	—	—	—	—	0.9	0.6	—	—	47.5	320
317–320 (ash)	—	—	—	33.8	13.5	0.3	—	4.5	0.0	—	—	—	—	0.6	—	—	—	47.3	334
320–335	—	—	0.3	26.6	17.0	2.2	2.2	5.4	0.3	—	—	—	—	—	—	—	—	45.8	312
335–350	—	—	—	15.4	6.3	1.5	0.9	7.5	0.9	—	—	—	0.3	—	—	—	—	67.2	332
350–370	—	—	—	19.4	16.1	8.1	1.6	8.7	0.3	0.3	—	—	—	—	—	—	—	45.5	310
370–378	—	—	0.3	20.3	12.9	21.5	11.1	17.5	0.3	0.3	—	—	0.3	0.6	—	—	—	14.8	325
378–450	—	—	—	3.9	4.9	0.4	0.5	3.4	0.3	—	—	—	0.1	0.2	—	—	—	86.4	1055
GC32, 0–19	—	—	—	19.4	15.9	3.4	0.6	6.3	0.0	—	—	—	—	—	—	—	—	54.4	320
19–35	—	—	0.6	16.8	7.9	8.6	4.4	25.1	1.0	0.3	0.3	0.3	—	1.3	—	—	—	33.3	315
35–185	—	—	—	9.6	5.1	4.8	2.6	17.3	4.2	0.3	—	—	—	1.3	0.6	0.3	—	54.0	313
185–320	—	—	0.3	28.7	10.7	4.3	3.7	10.4	0.6	—	—	—	—	0.3	—	0.3	—	40.9	328
320–345	—	—	0.3	15.3	8.8	5.9	3.1	20.6	2.2	—	—	—	—	0.9	—	0.6	—	42.2	320
345–360	—	—	—	18.9	5.9	10.6	8.6	23.9	0.6	0.3	—	—	0.3	1.8	0.9	—	0.3	28.0	339
360–380	—	—	0.3	19.1	9.5	2.5	1.2	2.5	0.0	—	—	—	—	—	0.3	—	—	64.6	325
380–441	—	—	—	19.6	10.4	7.3	1.3	12.3	2.2	—	—	—	0.3	—	0.3	—	—	46.4	317
441–517	—	—	—	24.1	9.6	6.2	4.0	17.0	0.3	0.3	—	—	—	0.3	—	—	—	38.1	323
517–520 (ash)	—	—	—	28.9	12.3	2.2	—	—	0.0	—	—	—	—	0.3	—	—	—	56.3	318
520–575	—	—	—	12.7	9.7	0.6	1.5	12.4	1.8	0.3	—	—	—	0.9	0.3	0.3	—	59.5	331
GC34, 0–14	—	—	—	13.1	12.8	4.7	1.2	3.4	0.0	—	—	—	—	—	—	—	—	64.8	321
14–60	—	—	0.3	25.0	14.9	16.2	4.6	19.8	1.2	—	—	—	—	—	—	—	—	18.0	328
60–98	—	0.3	—	25.9	13.1	8.3	3.4	16.0	0.3	—	0.3	—	—	0.3	0.6	—	—	31.6	351
98–100	—	—	0.0	36.8	19.3	0.3	—	4.3	0.0	—	—	—	—	—	—	—	—	39.3	326
100–200	—	—	0.0	22.9	16.2	7.4	2.9	10.3	0.6	—	—	—	—	0.9	0.3	—	—	38.5	340
200–260	—	—	0.3	24.8	10.7	28.5	7.1	12.3	0.9	—	0.3	—	—	0.6	0.3	—	—	14.1	326
260–337	—	—	1.5	11.2	7.1	3.8	1.5	11.8	3.6	0.3	—	—	—	0.3	0.3	0.3	—	58.3	338
337–420	—	—	0.3	18.4	8.7	5.4	2.4	12.0	0.6	—	0.3	0.3	—	0.3	—	0.0	—	51.2	332
360 (ash)	—	—	0.3	21.2	11.2	17.7	2.1	24.8	1.2	—	—	—	—	—	—	—	—	21.5	339

Table 3 (*continued*)

Site, interval in cm	Ol	Id	Cpx1	Cpx2	Opx	Hb	Am	Ep	Gm	Zr	Trm	St	Mon	Ap	Sph	Rt	Bi	Op	No.
420–578	—	—	0.3	14.5	8.1	7.4	1.6	11.0	3.5	—	—	0.3	—	0.3	0.3	0.3	—	52.3	310
578 (ash)	—	—	—	4.1	8.5	2.4	0.1	0.7	0.3	0.1	—	—	—	0.1	—	—	—	83.5	703
578–620	—	—	—	17.1	10.6	5.9	1.6	11.2	0.9	—	—	—	—	—	—	0.6	—	52.0	321
BC38, 0–15	—	0.3	—	19.8	12.2	9.6	1.0	2.6	0.3	—	—	—	—	—	—	—	0.3	53.8	303
15–30	—	—	—	15.3	11.6	5.6	2.0	7.0	1.0	—	—	0.3	—	—	—	—	—	57.1	301
30–65	—	—	—	25.4	11.3	12.5	3.2	5.1	1.3	—	—	—	—	—	—	—	0.6	40.5	311
GC39, 0–24	—	—	—	8.5	12.1	4.8	0.3	2.0	0.3	—	—	—	—	—	—	—	—	72.1	355
24–85	—	—	0.3	15.2	17.7	1.5	—	4.0	0.0	—	—	—	—	—	—	—	—	61.3	328
85–86	—	—	—	16.6	17.1	0.3	—	0.3	0.0	—	—	—	—	—	—	—	—	65.7	350
86–196	—	—	—	15.3	12.3	0.8	—	1.4	0.0	—	—	—	—	—	—	—	—	70.3	367
178–181	—	—	—	10.3	20.0	0.6	—	—	0.0	—	—	—	—	—	—	—	—	69.1	320
Vancouver Island area																			
PAN77-11	—	—	—	3.0	1.5	14.6	23.2	44.8	0.3	1.5	—	—	—	2.1	0.3	0.3	—	8.2	328
PAN77-25	—	—	—	2.2	0.6	26.0	16.2	39.7	1.6	1.6	—	—	—	0.6	—	—	—	11.4	315
PAN77-86	—	—	0.3	3.7	0.3	24.2	5.2	32.8	0.6	0.0	—	—	—	1.8	0.6	—	—	30.4	326
PAN77-107B	—	—	0.6	3.9	0.3	28.7	5.4	25.1	0.6	1.2	—	—	—	1.8	0.3	—	—	32.0	334
PAN78-44	—	—	—	2.2	0.3	24.1	9.0	25.3	0.9	1.9	—	—	—	0.6	—	0.3	—	35.5	324
PAN78-56	—	—	0.3	0.9	0.9	36.8	6.4	22.2	1.5	1.5	—	—	—	2.3	1.2	—	—	26.0	342
PAN78-59	—	—	0.6	3.1	1.2	35.2	8.0	28.7	0.6	1.2	—	—	—	3.1	—	—	—	18.3	327
PAR76-93	—	—	—	1.2	0.3	12.9	2.5	11.1	0.9	2.5	—	—	—	0.3	0.6	—	—	67.7	325
PAR86a-18	—	—	—	2.3	0.9	42.2	9.3	23.5	1.2	1.2	—	—	—	1.7	0.9	—	—	16.9	344
PAR86a-24	—	—	—	1.8	0.6	54.8	7.4	19.4	1.2	0.6	—	—	—	1.2	0.6	—	—	12.3	325
End78-3	—	—	0.3	2.0	1.1	20.3	8.3	50.6	2.6	0.3	—	—	—	1.4	—	—	—	13.1	350

Ol = olivine; Id = iddingsite; Cpx = clinopyroxene (1 = brown, 2 = green); Opx = orthopyroxene; Hb = brown and green amphibole; Am = pale and blue–green amphibole; Ep = epidote (group); Grn = garnet; Zr = zircon; Tm = tourmaline; St = staurolite; Mon = monazite; Ap = apatite; Sph = sphene; Rt = rutile; the other mineral symbols are in Table 2.

age (Fig. 7). Sediments from Site 16 (0–60 cm) are most likely to be Holocene.

Our dating is, to a marked degree, speculative. Nevertheless, we can infer with a high degree of certainty that the uppermost samples collected for mineral analyses from all our cores (see Tables 1–3) represent Holocene (post-glacial) sediments, whereas the samples taken below are of the Late Pleistocene–Holocene age (as glacial–interglacial).

4. Modern (post-glacial) North Pacific

The main feature of surface water circulation in the subarctic North Pacific is the cyclonic gyre with four cyclonic subgyres occupying the western and eastern parts in the open ocean, the Bering Sea and the Sea of Okhotsk (Dodiemead et al., 1963; Arsen'ev, 1968; Yasuoka, 1967; 1968; see Fig 1). Waters of the open ocean enter the marginal seas through central, eastern and northern passes in the island arcs separating the open and marginal North Pacific and exit through the western and southern passes. The water exchange is greatest in the Bering Sea where the passes are deeper and wider. To the northeast there is an extremely broad and shallow shelf over which the general flow of water is northward, passing finally through the Bering Strait and into the Chukchi Sea.

In both the marginal seas, mixing exists between the surface and deeper waters due to thermal convection (Bulgakov, 1975). Stable stratification is characteristic of the open ocean.

It is suggested that the open northwest Pacific Ocean receives deep water from the south, some of which penetrates into the marginal seas through the deepest passes in the island arcs. Intermediate water of low salinity is formed in the open North Pacific along the Subarctic Front (40–45°N) and then migrates southward following isopycnal surfaces (Reid, 1965; Kuksa, 1983). However, more recent data suggest that at least part of the North Pacific intermediate water mass is formed within the marginal seas, especially within the Sea of Okhotsk (Talley, 1991).

Clastic sedimentation in the deep parts of the marginal seas and in the trenches depends on turbidity currents, ice-rafting and, to a lesser degree, airborne and floating (pumice) pyroclastic transportation (Petelin, 1957; Aleksina, 1962; Lisitsyn, 1966; Creager et al., 1973; Knebel et al., 1974). In the open ocean, however, the latter mechanism dominates. Turbidite sediments appear only in the eastern part of the North Pacific where deep trenches surrounding the other parts of the region are absent, and ice-rafted detritus is not common outside the marginal seas (Horn et al., 1969; Kent et al., 1971; Creager et al., 1973; Stewart, 1976; Scholl et al., 1977). The present oceanographic or climatic conditions may be atypical as ice-rafting was very intensive in the open subarctic Pacific during the earlier periods of the Quaternary (Sancetta and Silvestri, 1984).

To determine the main sources of the clastic sediments, heavy mineral characteristics of the modern and, where there were few data, Pliocene–Pleistocene deposits from numerous areas on or in the vicinity of the possible provenances were compiled from Petelin (1957), Aleksina (1962), Lisitsyn (1966), Scheidegger et al. (1973), McManus et al. (1977) and Nechaev (1991) (Figs. 2 and 3). As a result, we can distinguish two main types of provenances, namely, volcanic and metamorphic. The volcanic provenances (VP) supply sediments usually with the arc-type volcaniclastics indicated by the association of orthopyroxene, green clinopyroxene and brown–green hornblende (Nechaev, 1991). The metamorphic provenances (MP) are characterized by high contents of pale colored and blue–green amphiboles, epidote (group), garnet, zircon, tourmaline, staurolite, monazite, andalusite and kyanite. It should be noted that brown–green hornblende belongs to both of the noted associations. The VP associations occupy parts of the Kuril–Kamchatka and Aleutian island arcs, whereas the MP associations are located in areas of the continental margins far from volcanic zones.

Most of the Holocene sediments sampled from the upper part of the cores contain the heavy mineral assemblages derived mainly from the volcanic provenances which are nearest to the sample locations (Fig. 2). There are only three exceptions (Sites 8, 9 and 16). The metamorphic detritus in the Site 16 diatomaceous clay may be interpreted

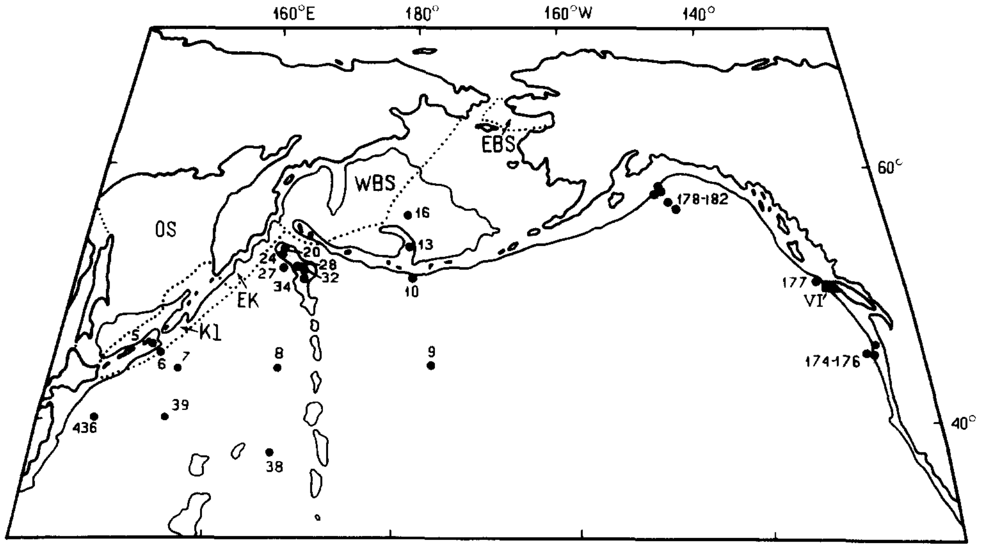

Fig. 2. Heavy mineral provinces of the modern northwest Pacific. *OS* = Sea of Okhotsk; *KI* = Kuril Islands; *EK* = eastern Kamchatka; *WBS* = western Bering Sea; *EBS* = eastern Bering Sea (generalized after Petelin, 1957; Aleksina, 1962; Lisitsyn, 1966; McManus et al., 1977).

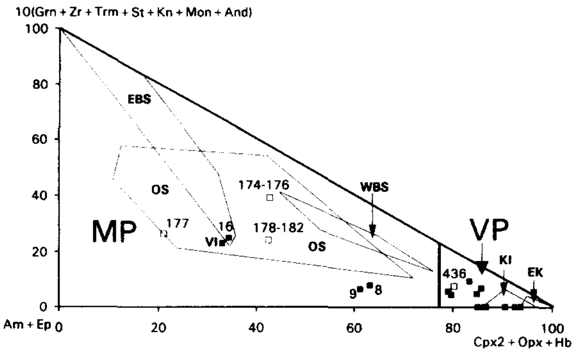

Fig. 3. Heavy mineral assemblages of Holocene sediments from the uppermost (Holocene) samples of the studied cores (closed rectangles) compared with average heavy mineral compositions of sediments deposited close to the possible provenances (fields and open rectangles, on the basis of data from Petelin, 1957; Aleksina, 1962; Lisitsyn, 1966; Scheidegger et al., 1973; McManus et al., 1977; Nechaev, 1991). The solid vertical line separates volcanic (*VP*) and metamorphic (*MP*) mineral suites. Numbers and letters indicate sites and provinces as shown on Fig. 2 (numbers of sites located inside the VP section are not displayed). Mineral abbreviations as in Table 3.

as transported by turbidity currents, but there is no evidence for this in the sedimentary structure. Hence the metamorphic association is most likely to be ice-rafted. Heavy mineral suites at Sites 8 and 9 are also related to ice-rafting because pelagic clays containing these suites include abundant erratic pebbles (see Table 1).

Our data suggest that at present ice-rafting affects pelagic sedimentation not only in the marginal seas but also in the open ocean. The modern North Pacific is not atypical in this respect. Unfortunately, the small number of heavy mineral analyses does not allow us to determine the exact sources of the metamorphic (ice-rafted) debris of the northwest Pacific.

5. Late Pleistocene (glacial) North Pacific

The growth of continental ice sheets during the last glaciation caused a global fall in sea level up to 100–120 m (Flint, 1971; Knebel et al., 1974; Williams et al., 1981; Fairbanks, 1989). As a result, large parts of the modern shelf areas were eliminated. This event was probably most dramatic in the Bering Sea where almost all the northeastern shelf including the Bering Strait, was exposed. On the surrounding land, glaciers covered mountains, whereas lowland areas were a tundra or steppe–tundra (Hopkins, 1972; Cwynar and Ritchie, 1980). Especially large lowland areas not covered by glaciers evidently existed on the exposed Bering Sea shelf.

The water mass exchange between the marginal seas and the open Pacific Ocean is proposed to have been more restricted than today, but deep passes such as those on the southwestern border of the Bering Sea and in the middle of the Kuril island arc were not closed or even significantly limited (Sancetta, 1983).

The general pattern of surface currents was similar to that of today (Kent et al., 1971; Sancetta, 1983). The greatest difference was an absence of the northward flow over the eastern Bering Sea into the Chukchi Sea. The straits between the Sea of Japan and the Sea of Okhotsk might also have been closed, resulting in colder conditions in the Sea of Okhotsk.

Data on the isotope compositions of benthic foraminifera suggest that during glacial times the formation of the intermediate water mass in the North Pacific and its southward migration were much more intensive than today. Even the upper deep water (up to 2600 m) was involved in this process (Duplessy et al., 1988; Gorbarenko, 1991). Mammerickx (1985) found evidence that the thermohaline flow transported fine-grained sediment southward from the Bering Sea and Sea of Okhotsk. However, Keigwin (1987) and Keigwin et al. (1992) found no carbon isotopic evidence for increased ventilation at 2980 m on Meiji Seamount in the northwestern corner of the open Pacific.

Ice-rafting was the principal mode of transportation for the coarse- and medium-grained clastics throughout the subarctic gyre during the glaciations. Its extension down to 40–45°N was indicated by the occurrence of coarse-grained erratic debris in the Late Pleistocene pelagic sediments. The main sources of the ice-rafted material are suggested to be icebergs derived from the Siberian and North American highland glaciers (Griggs and Kulm, 1969; Conolly and Ewing, 1970; Kent et al., 1971; von Huene et al., 1976; Sancetta and Silvestri, 1984).

To check these suggestions, we tried to define heavy mineral assemblages indicative of pelagic glacial debris, and their main provenances and distribution. Moreover, an attempt was made to understand how the productivity was linked to the change between glacial and interglacial conditions based on the contents of the diatom, radiolaria and foraminifer microfossils in the studied sediment fraction (0.05–0.1 mm).

As is shown in the left-hand graphs of Figs. 4–11, the heavy mineral compositions of the pelagic sediments fluctuate with time. We may distinguish two patterns among these changes. The first pattern is related to cores 13, 20, 24, 27, 28, 32 and, probably, 9, 10, 34 and 38 (the Bering Sea, Meiji and Detroit Seamounts, Aleutian

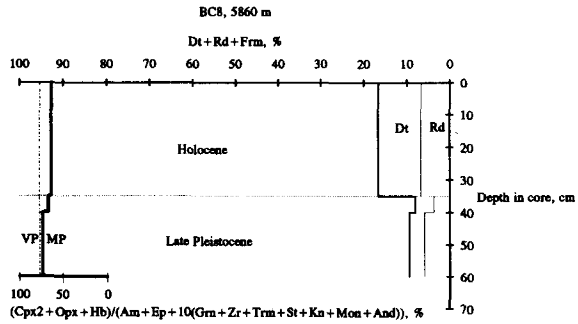

Fig. 4. Temporal changes in heavy mineral assemblages (left-hand graphs with the scale in the lower position) and total content of biofossils (right-hand graphs with the scale in the upper position) in core BC8 crossing the Holocene–Pleistocene boundary (horizontal broken line). The vertical broken line separates volcanic (*VP*) and metamorphic (*MP*) mineral suites. Mineral and biofossil abbreviations are as in Tables 2 and 3.

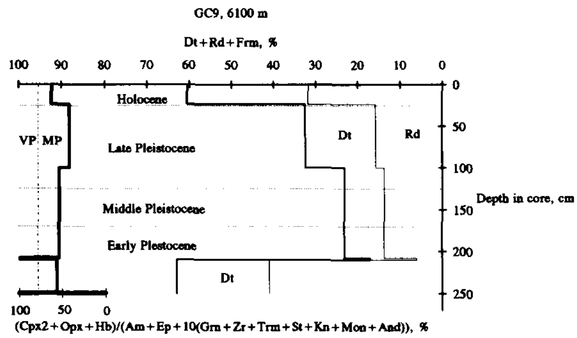

Fig. 5. Temporal changes in heavy mineral assemblages (left-hand graphs with the scale in the lower position) and total content of biofossils (right-hand graphs with the scale in the upper position) in core GC9 crossing the Holocene–Pleistocene boundary (horizontal broken line). The vertical broken line separates volcanic (*VP*) and metamorphic (*MP*) mineral suites. Mineral and biofossil abbreviations are as in Tables 2 and 3.

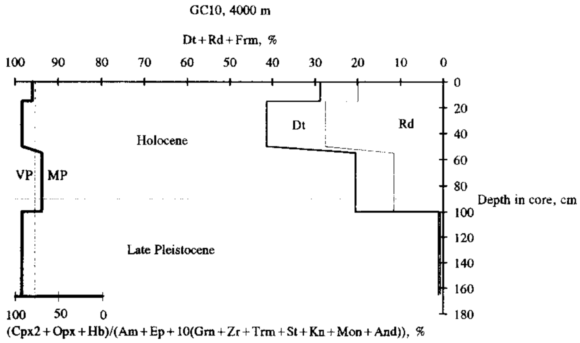

Fig. 6. Temporal changes in heavy mineral assemblages (left-hand graphs with the scale in the lower position) and total content of biofossils (right-hand graphs with the scale in the upper position) in core GC10 crossing the Holocene–Pleistocene boundary (horizontal broken line). The vertical broken line separates volcanic (*VP*) and metamorphic (*MP*) mineral suites. Mineral and biofossil abbreviations are as in Tables 2 and 3.

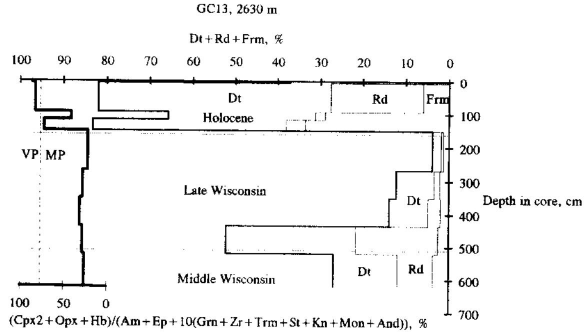

Fig. 8. Temporal changes in heavy mineral assemblages (left-hand graphs with the scale in the lower position) and total content of biofossils (right-hand graphs with the scale in the upper position) in core GC24 crossing the Holocene–Pleistocene boundary (horizontal broken line). The vertical broken line separates volcanic (*VP*) and metamorphic (*MP*) mineral suites. Mineral and biofossil abbreviations are as in Tables 2 and 3.

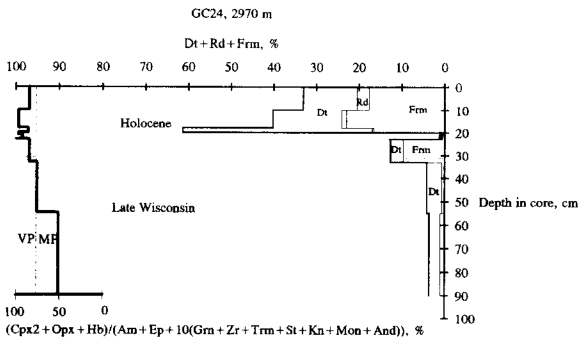

Fig. 7. Temporal changes in heavy mineral assemblages (left-hand graphs with the scale in the lower position) and total content of biofossils (right-hand graphs with the scale in the upper position) in core GC13 crossing the Holocene–Pleistocene boundary (horizontal broken line). The vertical broken line separates volcanic (*VP*) and metamorphic (*MP*) mineral suites. Mineral and biofossil abbreviations are as in Tables 2 and 3.

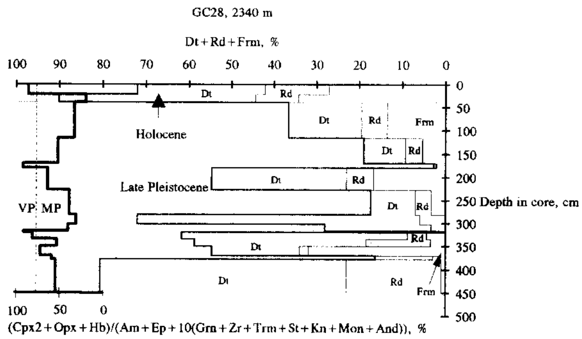

Fig. 9. Temporal changes in heavy mineral assemblages (left-hand graphs with the scale in the lower position) and total content of biofossils (right-hand graphs with the scale in the upper position) in core GC28 crossing the Holocene–Pleistocene boundary (horizontal broken line). The vertical broken line separates volcanic (*VP*) and metamorphic (*MP*) mineral suites. Mineral and biofossil abbreviations are as in Tables 2 and 3.

Trench and central North Pacific). Their heavy mineral assemblages indicate increased amounts of volcaniclastic material from the Late Pleistocene to Holocene. The second pattern is found in cores 7, 8 and 39, all from the Northwest Pacific Basin. In contrast with the previous cores, the mineralogy of these cores indicates a decrease in volcaniclastic material from the Late Pleistocene to Holocene.

The total content of biofossils in the studied cores (see Figs. 4–11) seems to reflect the uneven character of sediment supply related to volcanic input and ice-rafting. The most manifested minima of the biofossil content are associated with positive peaks of volcaniclastic material in ash layers. Other minima correspond to the maximum contents of metamorphic minerals near the Pleistocene–Holocene boundary (150–268 cm in GC13, 35–185 cm in GC32, 14–60 cm in GC34). In general, the relative amount of bioclasts increases from the Late Pleistocene to Holocene, although

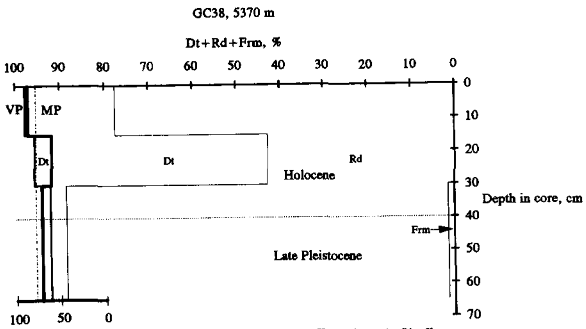

Fig. 10. Temporal changes in heavy mineral assemblages (left-hand graphs with the scale in the lower position) and total content of biofossils (right-hand graphs with the scale in the upper position) in core GC38 crossing the Holocene–Pleistocene boundary (horizontal broken line). The vertical broken line separates volcanic (*VP*) and metamorphic (*MP*) mineral suites. Mineral and biofossil abbreviations are as in Tables 2 and 3.

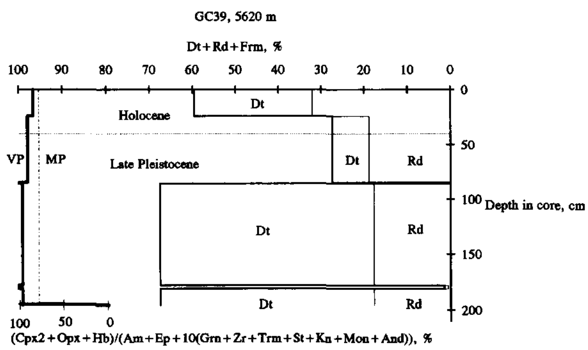

Fig. 11. Temporal changes in heavy mineral assemblages (left-hand graphs with the scale in the lower position) and total content of biofossils (right-hand graphs with the scale in the upper position) in core GC39 crossing the Holocene–Pleistocene boundary (horizontal broken line). The vertical broken line separates volcanic (*VP*) and metamorphic (*MP*) mineral suites. Mineral and biofossil abbreviations are as in Tables 2 and 3.

this tendency is overprinted by numerous fluctuations. It confirms the conclusions presented previously (Bezrukov and Romankevich, 1960; Jouse, 1960) that during glaciations, terrigenous sedimentation was dominant, whereas in post-glacial and interglacial times the deposition of biofossils was significant in the northwestern Pacific, including the marginal seas.

The increasing amounts of fine- and medium-grained terrigenous components in Late Pleistocene (glacial) deposits of the northern and central North Pacific are most likely due to ice-rafting because they are associated with coarse erratic detritus which is undoubtedly ice-rafted (Griggs and Kulm, 1969; Conolly and Ewing, 1970; Kent et al., 1971). To find the source of the terrigenous sediments we compared metamorphic heavy mineral assemblages from pelagic sediments with those of sediments from areas on and near possible provenances. The comparison was based on heavy mineral characteristics (the ratio between the contents of epidote and amphiboles versus the ratio between the contents of garnet and zircon), which were selected so that differences between the provenances were the best manifested (Fig. 12). As can be seen, the glacial sediments of the Northwest Pacific Ocean are closest in their heavy mineral assemblages to sediments of the eastern Bering Sea shelf (EBS provenance). Therefore, we infer that the eastern Bering Sea shelf was the main source of the ice-rafted material to the open Northwest Pacific. This conclusion is unexpected because the previous investigations proposed that the highland glaciers were the most important sources of icebergs carrying clastics into the region, whereas there was a large tundra area in the northeast Bering Sea during glacial times (see references cited above). With respect to these proposals, we, however, suggest that not icebergs but sea ice was the major transportation agent of ice-rafted material. There were evidently unique condi-

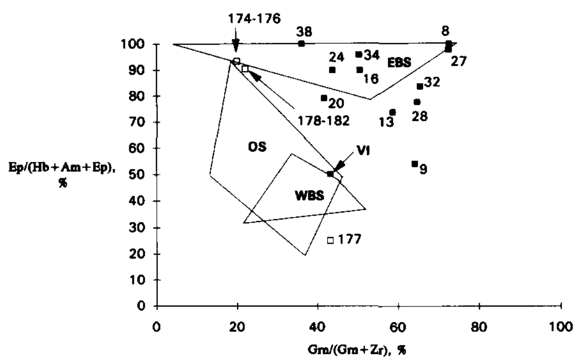

Fig. 12. Plot of average ratios Ep/(Hb+Am+Ep) and Grn/(Grn+Zr) in the North Pacific sediments with the dominant metamorphic heavy mineral assemblage (*MP*). Numbers and letters indicate sites and provinces as shown on Fig. 2.

tions for the generation of sea ice and its loading with abundant shelf detritus in the perfectly flat region of the northeast Bering Sea where spacious shallow water areas might freeze down to the bottom each winter and release the ice cover each summer. Perhaps such an environment exists on the modern Bering shelf but the northward water flow prevents the sea ice from moving into the open Pacific in marked amounts (see earlier).

There is no evidence for a terrigenous flux from the Sea of Okhotsk into the open Pacific in the studied Holocene–Pleistocene sediments, although those from Site 7 would best reflect such an influence if it indeed happened. We therefore have to infer that either ice-rafting, which might be the only agent for this transportation of material from the sea to the ocean, was never significant there or that the circulation of water in the sea was always too restricted.

The maximum content of metamorphic minerals in the transitional Pleistocene–Holocene sediments from the central Aleutian Trench (Fig. 6) may be related to the extreme ice-melting immediately after the Late Wisconsin glaciation. At that time, water currents from the Bering Sea might penetrate the open ocean through most of the passes between the Komandor and Aleutian islands, not only through the strait between Bering Island and Kamchatka as occurs now (compare Figs. 1 and 13).

The increasing contents of volcaniclastic material in the glacial sediments from cores 7, 8 and 39 may be explained by temporal changes in wind patterns and increasing volcanic activity. If any of these explanations is true, the Late Pleistocene sediments from cores 7, 8 and 39 would contain ash layers more often than those from other cores in the region. However, we noted only two ash layers in core 39 (cores 7 and 8 do not include any ash layers), which is common for the entire North Pacific. For example, we observed the similar frequency of ash layers in the Late Pleistocene sediments of the Meiji and Detroit Seamounts, which recorded the increasing input of metamorphic heavy minerals (see Table 1 and Figs. 8 and 9). Thus, the increasing volcanic contribution to the Late Pleistocene sediments of the southwestern North Pacific is most likely due to the drift of pumice with the Kuroshio water current that extended to the north further than today. This

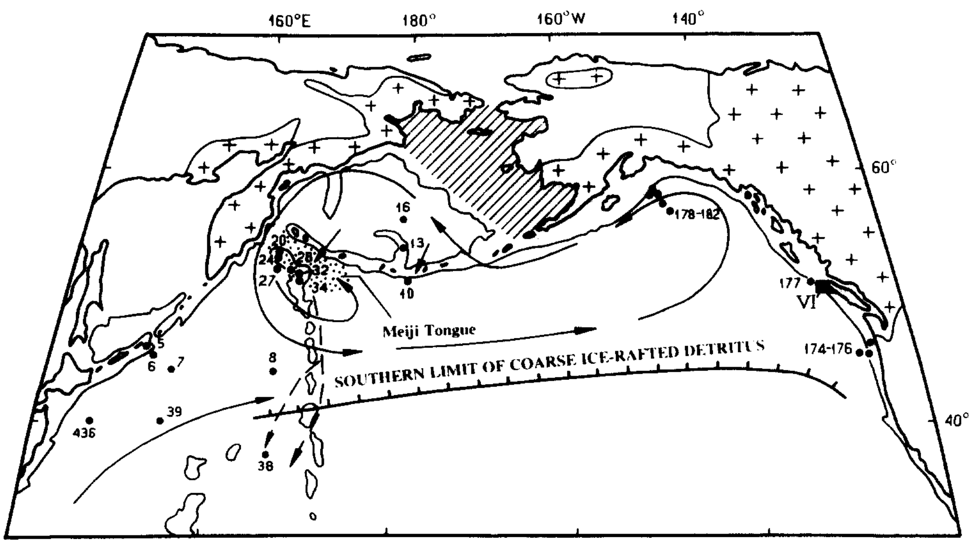

Fig. 13. Proposed scheme of ocean circulation in the Late Pleistocene North Pacific during glacial advances. The solid arrows indicate the surface water currents. The broken arrows indicate the proposed intermediate to deep water flow. The line-shaded area marks the main source of sea-ice highly loaded with terrigenous debris. The cross-shaded areas manifest highland regions covered by glaciers (after Hopkins, 1972). Southern limit of coarse ice-rafted detritus is shown after Griggs and Kulm (1969), Conolly and Ewing (1970) and Kent et al. (1971).

indicates the significant narrowing of the subarctic gyre in the latitudinal direction, which results in the focusing of its western subgyre over the northwestern Emperor Seamounts. Perhaps the Meiji Tongue, a thick pile of hemiterrigenous sediments located between the northwestern Emperor Seamounts and the Komandor island arc (Sites 20, 24, 28, 32 and 34; see Fig. 13), was formed because of that effect.

The increasing amount of metamorphic (ice-rafted) debris from the Holocene to Pleistocene sediments in core 38 (see Fig. 10), which was obtained from the eastern part of the North Pacific Basin at latitude 38°N, may be considered as conflicting with our previous suggestions. However, this conflict may be solved if we make the following speculations. During the glaciation, the large-scale generation of sea-ice in the Bering Sea produced dense water of low temperature and high salinity. The surface water currents then concentrated it in the area of the Meiji Tongue. These conditions created the southward flow of intermediate or deep water along the eastern flank of the Emperor chain as suggested by Mammerickx (1985). This flow penetrated the Northwest Pacific Basin in significant amounts only to the south of 45°N where there are relatively wide and deep passes between the seamounts (see Fig. 13).

If this is true, the increasing metamorphic debris in the 0.05–0.1 mm fraction from Holocene to Pleistocene sediments in core 38 indicates the influence of intermediate or deep water flow, which could not affect the sediments deposited to the west (Sites 7 and 39) and to the north (Site 8) of this location. Note that Site 38 is located to the south of the field of coarse ice-rafted detritus defined by Griggs and Kulm (1969), Conolly and Ewing (1970) and Kent et al. (1971). Our data support their definition as we have not found any coarse clasts in core 38, whereas they were abundant in cores 8 and 9 (see Table 1 and Fig. 13). Submarine currents probably carried the fine- and medium-grained debris further to the south than the coarse detritus. The proposed flow of intermediate or deep water is therefore confirmed by the extension of fine- and medium-grained debris beyond the southern limit of the coarse detritus.

6. Conclusions

Ice-rafting has had some influence on clastic sedimentation in the open subarctic Pacific throughout the Quaternary. This influence was most significant during the glacial advances and immediately following them, as was defined previously (Horn et al., 1969; Kent et al., 1971; Creager et al., 1973; Stewart, 1976; Sancetta and Silvestri, 1984). However, in contrast with the previous opinion suggesting that icebergs from the continental highlands were the major transportation agent of the ice-rafted detritus, our mineralogical data suggest that sea-ice, derived mainly from the northeastern Bering Sea shelf, provides the principal terrigenous flux to the open ocean.

Temporal and spatial changes in the relationship between volcanic and metamorphic heavy mineral assemblages in sediments support the previous idea that in the glacial epoch the intermediate and upper deep water formation in the northwest Pacific was more intensive than in post-glacial times. The thermohaline flow was probably initiated by focusing of the western subarctic gyre in the area of Meiji and Detroit Seamounts. It probably then extended southward, along the eastern slopes of the Emperor chain, and penetrated the Northwest Pacific Basin through passes between the seamounts to the south of 45°N.

It should be noted that mineralogical data might give more certain and reliable information for the paleo-oceanic study if they are based on detailed isotope stratigraphy. We hope that further cooperation between workers will allow this.

Acknowledgments

The investigation was carried out as a collaboration between Russian and American geologists as a part of the objective: "Clastic elements in modern sediments and their paleoceanic significance" of the GEMS (Geochemistry of Marine Sediments) Program initiated by Professor Mikhail F. Staschuk (now deceased) and co-ordinated by Drs Alexander S. Bychkov (Pacific Oceanological Institute, Russian Academy of Sciences) and James R. Hein (US Geological Survey).

We are grateful to all the participants of the *Vinogradov* cruise 19/4 for their help and cooperation. Special thanks are given to Charles Franks of the Woods Hole Oceanographic Institution, John Rapp of the US Geological Survey, Zinnat Badredinov, Eugene Mikhailik and Yuri Martynov (all of the Far East Geological Institute), with whom we had worked jointly on the deck.

We also thank Dr Lloyd D. Keigwin from Woods Hole Oceanographic Institution and the referees for their useful comments on this work, and Dr J. Vaugh Barrie and Trudie C. Forbes from the Geological Survey of Canada for the contributed samples.

References

Akiba, F., 1986. Middle Miocene to Quaternary diatom biostratigraphy in the Nankai Trough and Japan Trench, and modified Lower Miocene through Quaternary diatom zones for middle-to-high latitudes of the North Pacific. Init. Rep. DSDP, 87: 393–481.

Aleksina, I.A., 1962. Mineralogiya krupnoalevritovoy fraktsii donnykh osadkov Kronotskogo i Avachinskogo zalivov. Trudy Inst. Okeanol. SSSR, 61: 104–154.

Arsen'ev, V.S., 1967. Techeniya i vodnye massy Beningova morya. Nauka, Moscow, 133 pp.

Baldauf, J., 1982. Identification of the Holocene–Pleistocene boundary in the Bering Sea by diatoms. Boreas, 11: 113–118.

Bezrukov, P.L. and Romankevich, E.A., 1960. K stratigrafii i litologii donnykh otlojhenii severo-zapadnoi chasti Tikhogo okeana. Dok. SSSR, 130 (2): 417–420.

Broecker, W.S. and Denton, G.H., 1989. The role of ocean–atmosphere reorganizations in glacial cycles. Geochim. Cosmochim. Acta, 53: 2465–2501.

Broecker, W.S., Peteet, D.M. and Rind, D., 1985. Does the ocean–atmosphere system have more than one stable mode of operation? Nature, 315: 21–26.

Bulgakov, N.P., 1975. Konvektsiya v Okeane. Nauka, Moscow, 272 pp.

Conolly, J.R. and Ewing, M., 1970. Ice-rafted detritus in Northwest Pacific deep-sea sediments. Geol. Soc. Am. Mem., 126: 219.

Creager, J.S., Scholl, D.W. et al., 1973. Init. Rep. DSDP, 19, 913 pp.

Cwynar, L.C. and Ritchie, J.C., 1980. Arctic steppe-tundra: A Yukon perspective. Science, 208: 1375–1377.

Dodiemead, A.J., Favorite, F. and Hirano, T., 1963. Salmon of the North Pacific Ocean II—review of oceanography for the Subarctic Pacific Region. Int. N. Pacific Fisheries Commission, Bull., 13, 195 pp.

Duplessy, J.C., Shackleton, N.J., Fairbanks, R.G., Laberyrie, L., Oppo, D. and Kallel, N., 1988. Deep water source variations during the last climatic cycle and their impact on the global deep water circulation. Paleoceanography, 3 (3): 343–360.

Fairbanks, R.G., 1989. A 17,000-year glacio-eustatic sea level record: influence of glacial melting rates on the Younger Dryas event and deep-ocean circulation. Nature, 342: 637–642.

Flint, R.F., 1971. Glacial and Quaternary Geology. Wiley, New York, 892 pp.

Gorbarenko, S.A., 1991. O glubinnoi tsyrkulyatsyi Severo-Zapadnoi chasti Tikhogo okeana v poslednee oledenenie. Dok AN SSSR, 316: 979–983.

Griggs, G.B. and Kulm, L.D., 1969. Glacial marine sediments from the northeastern Pacific. J. Sedim. Petrol., 39: 1142–1148.

Hopkins, D.M., 1972. The paleogeography and climatic history of Beringia during late Cenozoic time. Internord, 12: 121–150.

Horn, D., Delach, M. and Horn, B., 1969. Distribution of volcanic ash layers and turbidites on the North Pacific. Geol. Soc. Am. Bull., 80: 1715–1724.

Jouse, A.P., 1960. Stratigraficheskiye i paleogeograficheskiye issledovaniya v severo-zapadnoi chasti Tikhogo okeana. Izd. SSSR, Moscow, 255 pp.

Keigwin, L.D., 1987. North Pacific deep water formation during the latest glaciation. Nature, 330: 362–364.

Keigwin, L.D., Jones G.A. and Froelich, P.N., 1992. A 15,000 year peleoenvironmental record from Meiji Seamount, far northwest Pacific. Earth Planet. Sci. Lett., 111: 425–440.

Kent, D., Opdyke, N.D. and Ewing, M., 1971. Climate change in the North Pacific using ice-rafted detritus as a climatic indicator. Geol. Soc. Am. Bull., 82: 2741–2754.

Knebel, H.J., Creager, J.S. and Echols, 1974. Holocene sedimentary framework, east-central Bering Sea continental shelf. In: Y. Herman (Editor), Marine Geology and Oceanography of the Arctic Seas. Springer, New York, pp. 157–172.

Kuksa, V.I., 1983. Promejhutochnye Vody Mirovogo Okeana. Hydrometeoizdat, Leningrad, 272 pp.

Lisitsyn, A.P., 1966. Recent Sedimentation in the Bering Sea. USSR Acad. Sci., Inst. Oceanology (English Translation: Israel Program for Scientific Translations, 1969), 614 pp.

Mammerickx, J., 1985. A deep sea thermohaline flow path in the northwest Pacific. Mar. Geol., 65: 1–19.

McManus, D.A., Kolla, V., Hopkins, D.M. and Nelson, C.H., 1977. Distribution of bottom sediments on the continental shelf, northern Bering Sea. Studies of the marine geology of the Bering Sea. U.S. Geol. Surv. Prof. Pap, 759-C, 31 pp.

Morley, J., Itays, J. and Robertson, J., 1982. Stratigraphic framework for the late Pleistocene in the northwest Pacific Ocean. Deep-Sea Res., 29 (12A): 1485–1499.

Nechaev, V.P., 1991. Evolution of the Philippine and Japan Seas from the clastic sediment record. Mar. Geo., 97: 167–190.

Petelin, V.P., 1957. Mineralogiya peschano-alevritovykh fraktsyi osadkov Okhotskogo morya. Trudy Inst. Okeanol. SSSR, 32: 77–138.

Reid, J.L., 1965. Intermediate waters of the Pacific Ocean. John Hopkins Oceanogr. Stud., 2, 85 pp.

Sancetta, C., 1983. Effect of Pleistocene glaciation upon oceanographic characteristics of the North Pacific Ocean and Bering Sea. Deep-Sea Res., 30 (8A): 851–869.

Sancetta, C. and Robinson, S., 1983. Diatom evidence on Wisconsin and Holocene events in the Bering Sea. Quat. Res., 20: 232–245.

Sancetta, C. and Silvestri, S., 1984. Diatom stratigraphy of the Late Pleistocene (Brunhes) Subarctic Pacific. Mar. Micropaleontol., 9: 263–274.

Scheidegger, K.F., Kulm, L.D. and Piper, D.J.W., 1973. Heavy mineralogy of unconsolidated sands in northeastern Pacific sediments: Leg 18, Deep Sea Drilling Project. Init. Rep. DSDP., 18: 877–887.

Scholl, D.W., Hein, J.R., Marlow, M.C. and Buffington, E.C., 1977. Meiji sediment tongue: North Pacific evidence for limited movement between the Pacific and North American plates. Geol. Soc. Am. Bull., 88: 1567–1576.

Stewart, R.J., 1976. Turbidites of the Aleutian abyssal plane: mineralogy, provenance and constraints for Cenozoic motion of the Pacific Plate. Geol. Soc. Am. Bull., 87: 793–808.

Talley, L.D., 1991. An Okhotsk Sea water anomaly: implication for ventilation in the North Pacific. Deep-Sea Res., 38, Suppl. 1: S171–S190.

von Huene, R., Crouch, J. and Larson, E., 1976. Glacial advance in the Gulf of Alaska area implied by ice-rafted material. Geol. Soc. Am. Mem., 145: 411–422.

Williams, D.F., Moore, W.S. and Fillon, R.H., 1981. Role of glacial Arctic Ocean ice sheets in Pleistocene oxygen isotope and sea level records. Earth Planet. Sci. Lett., 56: 157–166.

Yasuoka, T., 1967. Hydrography in the Okhotsk Sea (1). Oceanogr. Mag., 19: 61–72.

Yasuoka, T., 1968. Hydrography in the Okhotsk Sea (2). Oceanogr. Mag., 20: 55–63.